Geophysical Journal International

Geophys. J. Int. (2022) **228,** 2038–2047
Advance Access publication 2021 November 11
GJI Heat Flow and Volcanology

https://doi.org/10.1093/gji/ggab459

Feeding of a magma chamber by an ascending magma bubble

Michele Dragoni

Dipartimento di Fisica e Astronomia 'Augusto Righi', Alma Mater Studiorum, Università di Bologna, Viale Carlo Berti Pichat 8, 40127 *Bologna, Italy.*
E-mail: michele.dragoni@unibo.it

Accepted 2021 November 6. Received 2021 November 5; in original form 2021 July 23

SUMMARY

There is evidence that magma chambers are not fed by a continuous flow, but in the form of discrete magma batches. The possibility is considered that the chamber is fed by a magma bubble ascending through the region underneath, driven by buoyancy force. Due to the high ambient temperatures, it is assumed that the bubble moves through a viscoelastic medium with temperature-dependent viscosity. The motion of a spherical magma bubble and its inflow into the chamber are studied. The bubble volume is assumed to be at least equal to magma volumes in typical effusive eruptions on Mount Etna, corresponding to bubble radii of a few hundred metres. Under some simplifying assumptions, the problem is solved analytically. The bubble velocity is directly proportional to the square of its radius and inversely to the viscosity of surrounding rocks, but it is independent of magma viscosity. Velocity can reach values of the order of tens of metres per year in the proximity of the chamber. Since the characteristic time for heat diffusion is several hundred years, the bubble can cover several kilometres with only moderate cooling. During ascent, forced convection takes place in the bubble. Equations for convection streamlines are obtained and traveltimes of magma are calculated, giving a mixing time of the order of hundred years below the chamber. Inflow of the bubble in the magma chamber produces a pulse in flow rate. Under reasonable assumptions, pulse shape and duration are calculated analytically. Pulse duration can be several tens of years and can give rise to a sequence of eruptions, depending on the size of the bubble and the critical overpressure for eruption.

Key words: Effusive volcanism; Magma chamber processes; Physics of magma and magma bodies.

1 INTRODUCTION

Magma fluxes feeding magma chambers are difficult to ascertain, emphasizing the need for a better understanding of how magmatic systems evolve (e.g. Gudmundsson 2012). A challenging question is whether magma more commonly ascends during continuous or pulse-like flow. A variety of observations from plutonic and active systems suggest the prevalence of discrete pulses feeding reservoirs (Bons *et al.* 2004; Manea *et al.* 2005; Menand 2011). The occurrence of magma pulses has been inferred for the feeding of magma chambers prior to eruptions as well as for very long episodes of magma intrusion in the Earth's crust (Crisp 1984; Paterson & Vernon 1995; Scandone *et al.* 2007; Annen 2011; Michaut & Jaupart 2011). There are also thermal arguments for the episodic feeding of magma reservoirs: unless the crust is exceptionally hot, continuous magma feeding is incompatible with estimates of long-term-averaged filling rates (Menand *et al.* 2015).

Geophysical, geochemical and petrologic observations present a picture of magmatic systems that extend throughout the crust and are characterized by distributions of melt, crystals and exsolved volatiles that are heterogeneous in both space and time (Cashman *et al.* 2017). In general, magma ascent occurs via a combination of porous flow, diapirs and dikes, with ascent rate controlled by ambient conditions (Rubin 1993). In the upper crust, magma ascent occurs primarily via dikes, as numerous field outcrops attest.

This paper considers the particular region beneath a magma chamber, where the rheological properties may allow ascent via diapir-like structures. In this case, the possibility is explored that magma feeding magma chambers may flow in the form of discrete magma bubbles. Interesting questions are whether we can recognize distinct magma pulses and how far a magma bubble travelled from its source region to the magma chamber (Paterson *et al.* 2011).

The dynamics of ascending magma bubbles has been considered by several authors in connection with diapirism and the formation of plutons. Schmeling *et al.* (1988) considered a viscous sphere rising through another viscous fluid in order to represent the buoyant motion of a diapir. A review of previous work on the subject was given by Weinberg & Podladchikov (1994), who extended the model to non-Newtonian fluids.

Mass flow into a spherical magma chamber has been considered by Segall (2016), who assumed that flux is proportional to the difference between a constant source pressure and the magma chamber pressure. Currenti & Bonaccorso (2019) considered magma inflow into a spheroidal chamber during inter-eruptive periods, suggesting that they might be recorded by high-precision strain measurements.

In fact, transient variations in physical properties have been observed during magma ascent at Mount Etna (Patanè *et al.* 2006). The path of magma ascent may be defined by low values of the quality factor (De Gori *et al.* 2005) and it was shown that seismic attenuation of local earthquakes may strongly increase, announcing an incipient eruption (De Gori *et al.* 2011).

A time-varying injection rate and its effects on mass extraction have been considered by Karlstrom *et al.* (2012), who modelled stochastic dike flux that provides pulsed input to a magma chamber in a viscoelastic half-space. Degruyter & Huber (2014) proposed a model focused on the evolution of the thermodynamic state of the chamber as new magma is injected and showed how the frequency of eruptions depends on the timescale of injection.

Dragoni & Piombo (2020) assumed that an eruption is due to a magma pulse entering the chamber from the feeding system and showed that the finite duration of magma inflow may affect the time history of effusion rate. In the absence of data about possible pulse shapes, a simple bell-shaped function of time was chosen.

In the present paper, the ascent of a magma bubble through the region below the magma chamber is considered. The aim is to study the bubble dynamics in the final part of its ascent and to show that inflow in the chamber gives rise to a magma pulse that may be responsible for one or more eruptions. It must be noted that mass injection into a magma reservoir is not the only mechanism by which eruptions are triggered: a major role is played by the evolution of the thermodynamic state of the chamber (e.g. Degruyter & Huber 2014).

Although elastic behaviour well describes the uppermost layers of the Earth's crust, in active volcanic regions viscoelastic behaviour is more appropriate to characterize the medium around magma reservoirs, which can extensively perturb the geothermal gradient (Del Negro *et al.* 2009). Rocks surrounding a long-lived magmatic reservoir are heated significantly above the brittle–ductile transition and their behaviour is often modelled with a Maxwell viscoelastic rheology (e.g. Newman *et al.* 2001).

Accordingly, the region below the magma chamber is considered as a Maxwell viscoelastic medium through which a spherical bubble ascends driven by buoyancy force. This excludes the case in which the medium under the magma chamber is made of crystal mush, which has lower density than magma (Burgisser & Bergantz 2011). Pressurization of deeper magmatic reservoirs or exsolution of gas may be needed to drive magma ascent in this case.

The choice of a spherical shape is related to the possibility of solving the equations analytically, thus obtaining a deeper understanding of the underlying physics. Employing different shapes (such as a spheroid) for the bubble would not change sensibly the main results, in terms of relationships between bubble dynamics and rheological properties as well as the shape and duration of the associated magma pulse.

2 THE MODEL

We introduce a Cartesian coordinate system (x, y, z) and consider a spherical magma chamber with radius R_0 and centre at point $(0, 0, z_0)$ in the half-space $z < 0$. Let S_1 be the region below the magma chamber. We assume that S_1 is viscoelastic with density ρ_1 and a Maxwell rheology with viscosity η_1, rigidity μ_1 and characteristic time

$$\tau_1 = \frac{\eta_1}{\mu_1}. \tag{1}$$

We also consider a spherical magma body S_2 (hereafter called bubble), which is slowly rising through S_1 driven by buoyancy force, with velocity

$$\mathbf{u} = u\hat{\mathbf{z}}. \tag{2}$$

Let R_2 be the radius, ρ_2 the density and η_2 the viscosity of the bubble, with $R_2 \ll R_0$. Let $\mathbf{x}_2(t)$ be the position of the bubble centre at time t (Fig. 1). We define a characteristic ascent time, equal to the time the bubble takes to cover a distance equal to its diameter:

$$\tau_2 = \frac{2R_2}{u}. \tag{3}$$

Density in the region is then

$$\rho(\mathbf{x}, t) = \begin{cases} \rho_1, & \mathbf{x} \in S_1 \\ \rho_2, & \mathbf{x} \in S_2 \end{cases} \tag{4}$$

with $\rho_1 > \rho_2$, producing a buoyancy force

$$\mathbf{f} = (\rho - \rho_1)\mathbf{g}, \tag{5}$$

where $\mathbf{g}$ is the acceleration of gravity. Viscosity is

$$\eta(\mathbf{x}, t) = \begin{cases} \eta_1, & \mathbf{x} \in S_1 \\ \eta_2, & \mathbf{x} \in S_2 \end{cases}. \tag{6}$$

Viscosity η_1 is a function of temperature T that will be evaluated from the Arrhenius formula

$$\eta_1(T) = De^{\frac{E}{RT}}, \tag{7}$$

where D is the Dorn parameter, E is the activation energy and R is the gas constant (e.g. Ranalli 1995). For viscosity η_2, a typical value of high-temperature basaltic magmas will be assumed.

Temperature in region S_1 is dominated by the presence of magma chamber. The perturbation due to the bubble is neglected. In steady-state conditions, the heat equation is

$$\kappa\nabla^2 T + H = 0, \tag{8}$$

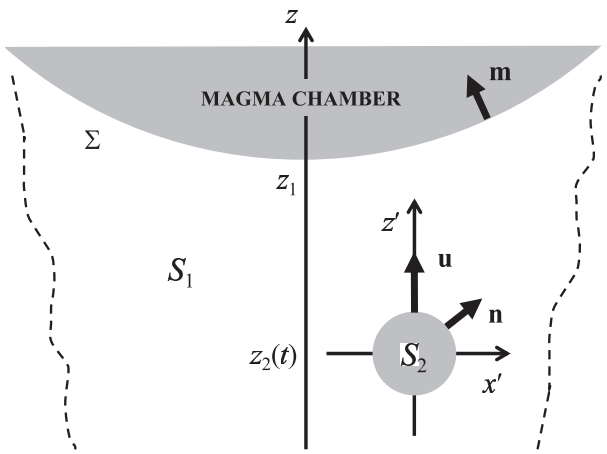

Figure 1. Sketch of the model. The magma chamber lies in the half-space $z < 0$. The Earth's surface is at $z = 0$. The centre and the bottom of the chamber are at $z = z_0$ and $z = z_1$, respectively. At a generic time t, the centre of the rising bubble is at $z = z_2(t)$.

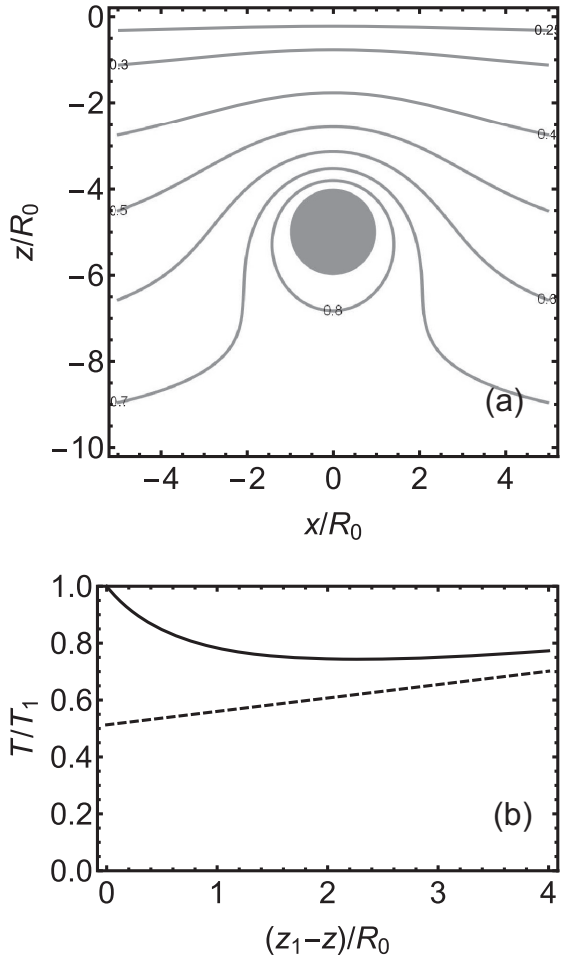

Figure 2. (a) Temperature field $T(x, z)/T_1$ around a spherical magma chamber with radius R_0 and centre at $z = z_0$; (b) temperature $T(z)/T_1$ on the z-axis below the magma chamber. The dashed line is the unperturbed crustal geotherm ($z_0 = -5R_0$, $T_1 = 1273$ K, $T_s = 293$ K, $k = 30$ K km^{-1}). Bottom of magma chamber is at $z = z_1$.

where κ is the thermal conductivity of S_1 and H is the heat production of the magma chamber. Temperature can be considered as the superposition of a typical crustal geotherm and the temperature field generated by the chamber. A solution of eq. (8) satisfying boundary conditions $T = T_s$ at the Earth's surface $z = 0$ and $T = T_1$ at the bottom of the chamber $(0, 0, z_1)$ is

$$T(\mathbf{x}) = T_s - kz + (T_0 - T_s + kz_1)R_0\left(\frac{1}{r_1} - \frac{1}{r_2}\right), \tag{9}$$

where k is the unperturbed geothermal gradient,

$$r_1 = \sqrt{x^2 + y^2 + (z - z_0)^2}, \qquad r_2 = \sqrt{x^2 + y^2 + (z + z_0)^2} \tag{10}$$

and

$$T_0 = \frac{|z_1 + z_0|T_1 - |z_1 - z_0|(T_s - kz_1)}{|z_1 + z_0| - |z_1 - z_0|}. \tag{11}$$

A contour plot of the ratio T/T_1 on the plane $y = 0$ is plotted in Fig. 2(a). It can be seen that T is laterally uniform to a good approximation in region S_1. Temperature on the z-axis below the chamber ($z \le z_1$) can be written as

$$T(z) = T_s - kz - (T_1 - T_s + kz_1)R_0\frac{z_1 + z_0}{z^2 - z_0^2} \tag{12}$$

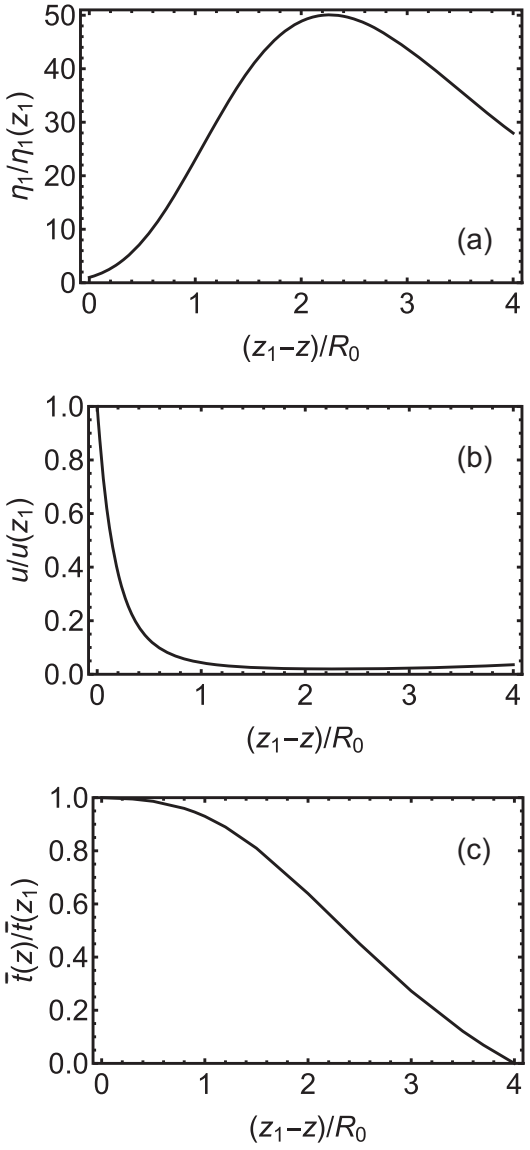

Figure 3. (a) Viscosity η_1 of region S_1; (b) upward velocity u of the magma bubble and (c) traveltime $\bar{t}$ of the bubble, as functions of distance $z_1 - z$ from the bottom of the magma chamber at $z = z_1$ ($\bar{t} = 0$ at $z = z_1 - 4R_0$).

and is plotted in Fig. 2(b). As a function of depth, T is approximately constant, apart from the vicinity of the chamber.

In order to estimate the orders of magnitude of quantities involved in the problem, we assume a value $R_0 = 2$ km for the radius of the magma chamber and $R_2 = 200$ m for the radius of the bubble. Viscosity η_1 is calculated according to eq. (7) with Dorn parameter $D = 10^9$ Pa s, activation energy $E = 120$ kJ mol^{-1} (Kirby & Kronenberg 1987; Del Negro *et al.* 2009) and $R = 8.31$ J mol^{-1} K^{-1}.

If we assume a temperature $T_1 = 1273$ K at the bottom of the magma chamber $z = z_1$, it results $\eta_1(z_1) \simeq 10^{14}$ Pa s. With $\mu_1 = 10^{10}$ Pa, the Maxwell time is $\tau_1 \simeq 10^4$ s. As shown in Fig. 3(a), values of η_1 increase with depth below the chamber (by a factor of 50 at a distance just greater than $2R_0$ from the chamber bottom) and then decrease. Accordingly, bubble motion is very slow: for most of the path, a value of u of the order of 1 m a^{-1} is obtained (Fig. 3b), entailing a characteristic ascent time τ_2 equal to about 20 a. Then

$\tau_2 \gg \tau_1$, so that bubble motion takes place as if the surrounding medium were a viscous liquid.

Since bubble temperature is higher than the temperature of surrounding rocks, the bubble is subject to cooling during its motion. The characteristic cooling time for heat diffusion is

$$\tau_3 = \frac{R_2^2}{4\chi}, \tag{13}$$

where χ is thermal diffusivity. With $\chi = 10^{-6}$ m^2 s^{-1}, it results $\tau_3 = 10^{10}$ s or about 300 a, so that $\tau_3 \gg \tau_2$. A greater contribution to cooling is given by forced convection inside the bubble, which will be considered in Section 4. The relative importance of advection with respect to diffusion is given by the Péclet number

$$P\acute{e} = \frac{u R_2}{\chi} \tag{14}$$

that is of the order of 10^2 in the proximity of the chamber. However, convection is very slow as well (an overturn time τ_4 equal to $5\tau_2$ will be found), so that cooling rate remains small. Cooling entails a very slow increase in bubble viscosity η_2 during ascent. We assume that η_2 is of the order of 10^2 or 10^3 Pa s, typical of high-temperature basaltic magmas.

The problem of bubble motion is solved by a procedure similar to that used by Landau & Lifshitz (1987), who considered a viscous liquid drop falling through a liquid with different viscosity. We introduce a coordinate system (x', y', z') in which the bubble is stationary, defined as

$$\mathbf{x}' = \mathbf{x} - \mathbf{x}_2. \tag{15}$$

In this system, viscosity η_1 can be considered spatially uniform, but slowly increasing with time, with a rate

$$\frac{\partial \eta_1}{\partial t} = \frac{\partial \eta_1}{\partial z} u \tag{16}$$

that is a very small quantity due to the slowness of bubble motion. As to viscosity η_2, it can also be considered slowly increasing in time due to cooling, but uniform due to convection.

Accordingly, we assume that both regions S_1 and S_2 are homogeneous and isotropic. We also assume that they are incompressible. Then the equation of motion is the Navier–Stokes equation. A steady-state motion with small Reynolds number is considered, due to the small velocity and the high viscosities. Under these assumptions, the equation reduces to

$$\eta \nabla^2 \mathbf{v}' - \nabla p' + \mathbf{f} = 0, \tag{17}$$

where $\mathbf{v}'$ is the flow velocity and p' is the variation of pressure with respect to equilibrium conditions. The continuity equation is

$$\nabla \cdot \mathbf{v}' = 0. \tag{18}$$

3 FLOW VELOCITY

Eqs (17) and (18) must be solved separately for the two regions S_1 and S_2. To this aim, boundary conditions must be assigned at the bubble surface. During the motion, the bubble surface undergoes a small change in shape, due to pressure differences. This change is a higher order effect and can be neglected (Landau & Lifshitz 1987).

Therefore boundary conditions can be imposed on the spherical surface. They are: vanishing of normal components of velocity of the inner and outer liquid; continuity of tangential component of velocity; continuity of normal and tangential components of stress. They provide five equations allowing us to determine constants a_1, b_1, a_2, b_2 and u appearing in the solution.

In region S_1, the flow velocity is

$$\mathbf{v}' = a_1 \frac{\mathbf{u} + \hat{\mathbf{n}}(\mathbf{u} \cdot \hat{\mathbf{n}})}{r} + b_1 \frac{\mathbf{u} - 3\hat{\mathbf{n}}(\mathbf{u} \cdot \hat{\mathbf{n}})}{r^3} - \mathbf{u}, \tag{19}$$

where $\hat{\mathbf{n}}$ is the unit normal vector to the bubble surface and

$$r = \sqrt{x'^2 + y'^2 + z'^2}. \tag{20}$$

The constants are

$$a_1 = \frac{2 + 3\gamma}{4(1 + \gamma)} R_2, \qquad b_1 = \frac{\gamma}{4(1 + \gamma)} R_2^3 \tag{21}$$

with

$$\gamma = \frac{\eta_2}{\eta_1}. \tag{22}$$

In the bubble interior (region S_2), the flow velocity is

$$\mathbf{v}' = a_2 \mathbf{u} + b_2 r^2 [\hat{\mathbf{n}}(\mathbf{u} \cdot \hat{\mathbf{n}}) - 2\mathbf{u}], \tag{23}$$

where

$$a_2 = \frac{1}{2(1 + \gamma)} \qquad b_2 = \frac{1}{2R_2^2(1 + \gamma)}. \tag{24}$$

The bubble velocity is

$$u = \frac{2R_2^2 g(\rho_1 - \rho_2)(1 + \gamma)}{3\eta_1(2 + 3\gamma)}. \tag{25}$$

Since $\gamma \ll 1$, it will be neglected henceforth. Therefore, eq. (25) reduces to

$$u = \frac{R_2^2 g(\rho_1 - \rho_2)}{3\eta_1} \tag{26}$$

that retrieves Stokes' solution for a solid body rising or falling through a viscous liquid (e.g. Batchelor 1967). A graph of $u(z)$ is given in Fig. 3(b), showing an acceleration of motion in the proximity of magma chamber. Upon substitution of eq. (26) in eq. (3), the characteristic ascent time becomes

$$\tau_2 = \frac{6\eta_1}{R_2 g(\rho_1 - \rho_2)}. \tag{27}$$

In the reference system of the Earth's crust, we can calculate the time $\bar{t}(z)$ taken by the bubble to rise up to a given depth z. Supposing that the bubble centre is at point $(0, 0, z_3)$ at time $t = 0$, the traveltime is

$$\bar{t}(z) = \int_{z_3}^{z} \frac{\mathrm{d}z^*}{u(z^*)} \tag{28}$$

or, thanks to eqs (26) and (7),

$$\bar{t}(z) = \frac{3D}{R_2^2 g(\rho_1 - \rho_2)} \int_{z_3}^{z} \mathrm{e}^{\frac{E}{RT(z^*)}} \, \mathrm{d}z^*, \tag{29}$$

where $T(z^*)$ is given by (12) with $z = z^*$. The integral must be solved numerically and the result is shown in Fig. 3(c), where $\bar{t}$ has been plotted for $z_3 = z_1 - 4R_0$. The graph also yields the position $z_2(t)$ of the bubble as a function of time during its ascent: z_2 increases almost linearly up to $t = 0.8\,\bar{t}(z_1)$, then it shows an acceleration up to the base of the chamber.

The flow inside and outside the bubble has axial symmetry around the z' axis. Therefore, it can be plotted in the plane $y' = 0$, where

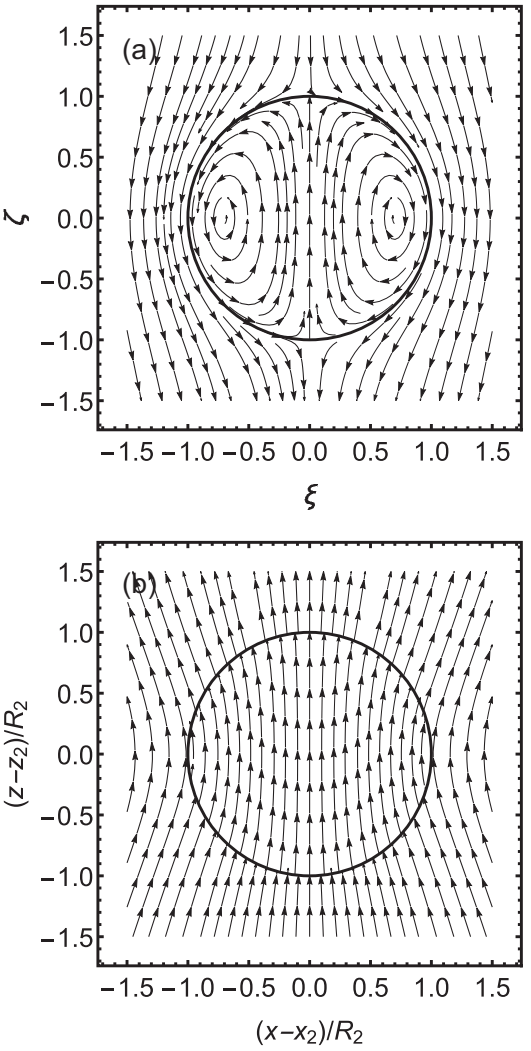

Figure 4. (a) Flow velocity $v'(\xi, \zeta)$ inside and around the magma bubble in the reference system of the bubble; (b) flow velocity $v(x, z)$ inside and around the bubble in the reference system of the Earth's crust.

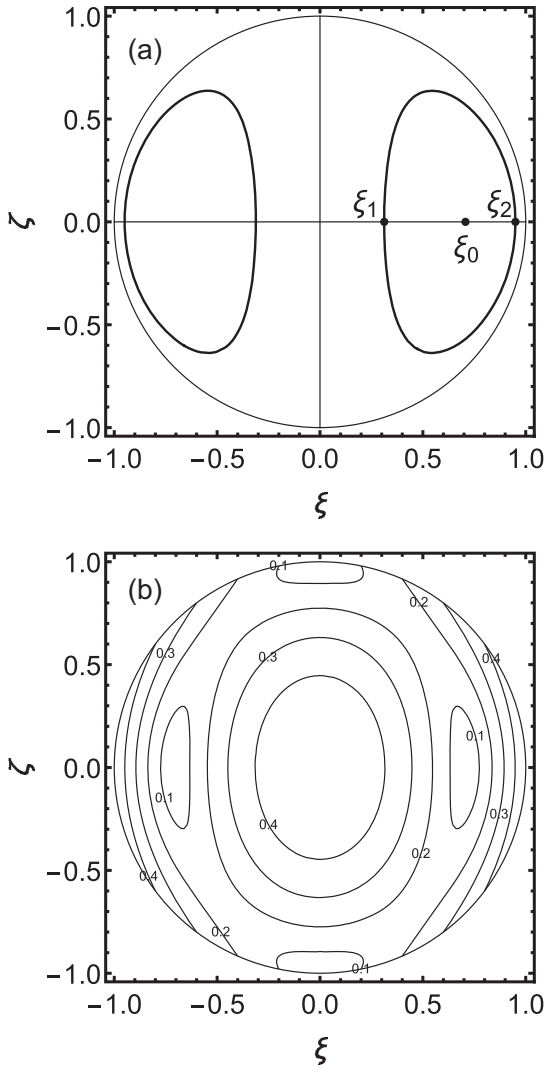

Figure 5. (a) Symmetric streamline loops in the bubble, corresponding to $\xi_2 = 0.95$; (b) magnitude $v'(\xi, \zeta)/u$ of flow velocity in the bubble.

the v'_y component of velocity vanishes. From eq. (19) the velocity components in region S_1 are

$$v'_x = \frac{x'z'}{r^3}\left(a_1 - \frac{3b_1}{r^2}\right)u \tag{30}$$

$$v'_z = -\left[1 - \frac{z'^2}{r^3}\left(a_1 - \frac{3b_1}{r^2}\right) - \frac{1}{r}\left(a_1 + \frac{b_1}{r^2}\right)\right]u. \tag{31}$$

From eq. (23), the velocity components in region S_2 are

$$v'_x = b_2 x' z' u \tag{32}$$

$$v'_z = (a_2 - 2b_2 r^2 + b_2 z'^2)\, u. \tag{33}$$

Flow velocity inside and outside the bubble is plotted in Fig. 4(a) as a function of non-dimensional coordinates:

$$\xi = \frac{x'}{R_2}, \qquad \zeta = \frac{z'}{R_2}. \tag{34}$$

In the reference system of the Earth's crust, flow velocity is given by

$$\mathbf{v}(\mathbf{x}) = \mathbf{v}'(\mathbf{x} - \mathbf{x}_2) + \mathbf{u} \tag{35}$$

and is shown in Fig. 4(b).

4 FORCED CONVECTION IN THE BUBBLE

A consequence of bubble motion is that magma is subject to forced convection. Magma close to the bubble surface is dragged downward during ascent, while it rises in the central part of the bubble. The equation of streamlines in the plane $\xi\zeta$ is

$$\frac{\mathrm{d}\xi}{\mathrm{d}\zeta} = \frac{v'_x}{v'_z}. \tag{36}$$

Upon substitution of eqs (32) and (33) and use of eq. (34), we obtain the differential equation

$$\frac{\mathrm{d}\xi}{\mathrm{d}\zeta} = \frac{\xi\zeta}{1 - 2\xi^2 - \zeta^2} \tag{37}$$

that has the solution

$$\xi^2(1 - \xi^2 - \zeta^2) = \xi_1^2\xi_2^2, \tag{38}$$

representing a quartic curve made of two disconnected loops that are symmetric with respect to the ξ and ζ axes (Fig. 5a). The loop in the half-plane $\xi > 0$ intersects the ξ axis at points $(\xi_1, 0)$ and

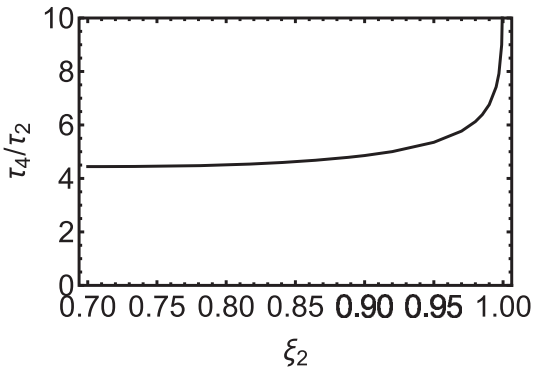

Figure 6. Traveltime τ_4 of magma along streamlines as a function of streamline parameter ξ_2, ranging from $\xi_0 = 1/\sqrt{2}$ to 1.

$(\xi_2, 0)$ such that

$$\xi_1^2 + \xi_2^2 = 1. \tag{39}$$

They are the minimum and the maximum distance of the streamline from the origin, respectively. All streamlines are generated by varying one of the two parameters ξ_1 or ξ_2 over its own range, that is

$$0 < \xi_1 < \xi_0, \qquad \xi_0 < \xi_2 < 1, \tag{40}$$

where

$$\xi_0 = \frac{1}{\sqrt{2}}. \tag{41}$$

All streamlines enclose the point $(\xi_0, 0)$, where velocity vanishes. The traveltime along a streamline C is

$$\tau_4 = \int_C \frac{\mathrm{d}s}{v'}, \tag{42}$$

where $\mathrm{d}s$ is the infinitesimal line element and v' is the magnitude of $\mathbf{v}'$:

$$v'(\xi, \zeta) = \frac{u}{2}\sqrt{\xi^2\zeta^2 + (1 - 2\xi^2 - \zeta^2)^2}. \tag{43}$$

A contour plot of v' is shown in Fig. 5(b). Thanks to the symmetry of streamlines with respect to the plane $\zeta = 0$, we can write

$$\tau_4 = 2R_2 \int_{\xi_1}^{\xi_2} \frac{\mathrm{d}\xi}{v'_\xi}, \tag{44}$$

where, thanks to eqs (32), (34), (38) and (39),

$$v'_\xi = \frac{u}{2}\sqrt{(\xi^2 - \xi_1^2)(\xi_2^2 - \xi^2)}. \tag{45}$$

Then,

$$\tau_4 = 2\tau_2 \int_{\xi_1}^{\xi_2} \frac{\mathrm{d}\xi}{\sqrt{(\xi^2 - \xi_1^2)(\xi_2^2 - \xi^2)}}, \tag{46}$$

where the characteristic ascent time (3) has been introduced. Integration yields

$$\tau_4 = \frac{2\tau_2}{\xi_2} K\left(\frac{\sqrt{\xi_2^2 - \xi_1^2}}{\xi_2}\right), \tag{47}$$

where K is the complete elliptic integral of the first kind (e.g. Abramowitz & Stegun 1972). The ratio τ_4/τ_2 is shown in Fig. 6 as a function of the streamline parameter ξ_2 and is equal to about 5 for all streamlines. The time τ_4 can be considered as the mixing time of magma in the bubble. There is complete mixing after a run approximately equal to 10 times the bubble radius R_2, independently of bubble velocity.

5 INFLOW INTO THE MAGMA CHAMBER

In a previous paper (Dragoni & Piombo 2020) it was shown that feeding of a magma chamber by a magma pulse may explain the observed time histories of effusion rate, in the case of eruption. A bell-shaped function of time was employed for the pulse, while pulse duration was chosen in order that it was comparable with the duration of an eruption. Here it is shown that the shape and duration of a magma pulse can be obtained as the result of a magma bubble entering the chamber.

Let Σ be the surface of the magma chamber. We suppose that the bubble touches Σ at point P and time $t = t_0$. The magma flow rate entering the chamber is

$$\Phi(t) = \int_\Pi \mathbf{u} \cdot \mathbf{m}\, \mathrm{d}S, \tag{48}$$

where $\mathbf{m}$ is the unit normal to Σ and Π is the intersection of Σ with the bubble S_2. Since $R_0 \gg R_2$, we neglect the curvature of Σ and consider the tangent plane to Σ at P. Then Π is a disk with radius $r_0(t)$ for $t > t_0$.

During magma inflow, forces acting on the bubble change, entailing a change in bubble velocity and a possible deformation of the bubble. When the bubble enters the magma chamber, eq. (26) no longer holds, but flow velocity is still controlled by buoyancy force, that decreases as the bubble penetrates into the chamber, because the density contrast between the two magmas vanishes.

These complications do not change the pulse-like shape of flow rate and we assume, for the sake of simplicity, that the bubble velocity decreases linearly to zero: this makes it possible to obtain a simple analytical expression for inflow rate. The time required for inflow of the entire bubble is then

$$\tau_5 = 2\tau_2 \sec\alpha, \tag{49}$$

where α is the angle between vectors $\mathbf{u}$ and $\mathbf{m}$. Introducing a non-dimensional time

$$t' = \frac{t - t_0}{\tau_5}, \tag{50}$$

we write

$$\mathbf{u}(t') = u_0(1 - t')\,\hat{\mathbf{z}}, \quad 0 \le t' \le 1, \tag{51}$$

where u_0 is the velocity at $t = t_0$. Then, eq. (48) yields

$$\Phi(t') = \pi u_0 \cos\alpha (1 - t') r_0^2 \tag{52}$$

or, thanks to eq. (49),

$$\Phi(t') = \frac{4\pi R_2}{\tau_5}(1 - t')h(2R_2 - h), \tag{53}$$

where h is the height of the spherical cap entering the chamber:

$$h(t') = \tau_5 \cos\alpha \int_0^{t'} u(t^*)\mathrm{d}t^* \tag{54}$$

whence

$$h(t') = 2R_2\, t'(2 - t'). \tag{55}$$

Then,

$$\Phi(t') = 12\frac{V_2}{\tau_5}\, t'(2 - t')(1 - t')^3, \tag{56}$$

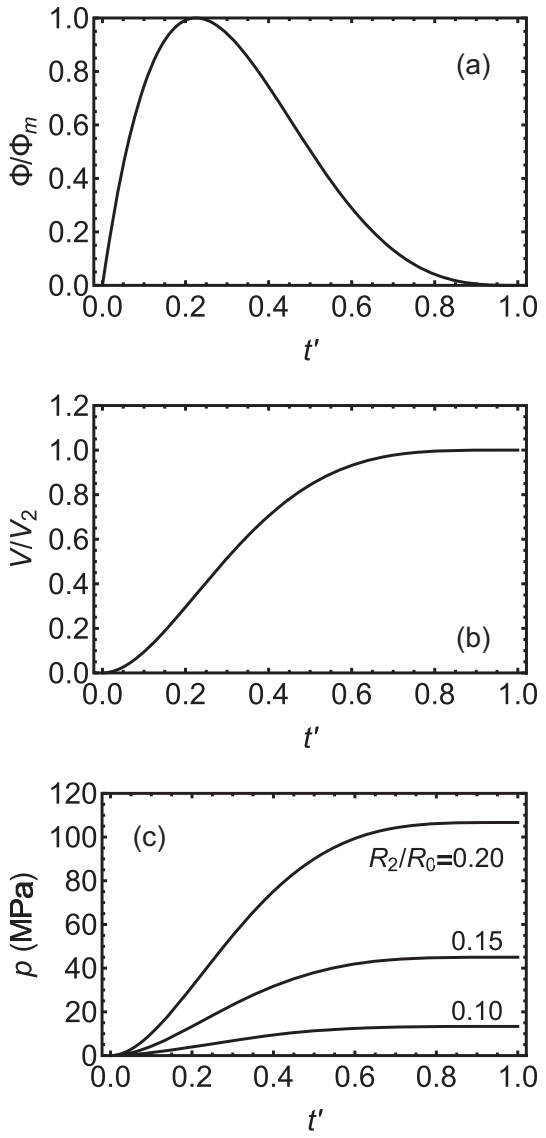

Figure 7. (a) Flow rate $\Phi(t')$ of the magma pulse and (b) cumulative volume $V(t')$ entering the magma chamber as functions of non-dimensional time t'; (c) pressure induced in the chamber as a function of t' for different values of the ratio R_2/R_0 in the absence of eruptions ($\mu_1 = 10^{10}$ Pa).

where V_2 is the volume of the bubble. It is easy to find that the maximum flow rate Φ_m is attained at time

$$t'_m = 1 - \sqrt{\frac{3}{5}} \tag{57}$$

and its value is

$$\Phi_m = 8\left(\frac{3}{5}\right)^{5/2}\frac{V_2}{\tau_5}. \tag{58}$$

The ratio $\Phi(t')/\Phi_m$ is shown in Fig. 7(a), showing an asymmetric pulse. The cumulative volume entering the chamber is

$$V(t') = \tau_5 \int_0^{t'} \Phi(t^*)\,\mathrm{d}t^*. \tag{59}$$

Introducing eq. (56) and integrating, we obtain

$$V(t') = V_2 \begin{cases} t'^2(2-t')^2(3-4t'+2t'^2), & 0 \le t' \le 1 \\ 1, & t' > 1. \end{cases} \tag{60}$$

A graph of the ratio $V(t')/V_2$ is shown in Fig. 7(b).

The overall deformation of the magma chamber following bubble inflow involves the rheological behaviour of the entire crust, also above the chamber and laterally to it, where temperatures are lower and viscosities are higher than in region S_1. In particular, above the chamber, temperature decreases rapidly from T_1 to T_s and the average viscosity is orders of magnitude greater. Therefore an elastic behaviour is assumed for this overall deformation.

According to eq. (49), τ_5 has the same order of magnitude as τ_2, that is tens of years. If we assume that the Earth's crust behaves elastically over times of the order of τ_5, the pressure increase produced in the chamber by magma inflow is (Dragoni & Piombo 2020)

$$p(t') = k_1\rho_2 V(t'), \tag{61}$$

where

$$k_1 = \frac{\mu_1}{\pi\rho_2 R_0^3}. \tag{62}$$

Hence,

$$p(t') = p_m \begin{cases} t'^2(2-t')^2(3-4t'+2t'^2), & 0 \le t' \le 1 \\ 1, & t' > 1 \end{cases} \tag{63}$$

where

$$p_m = \frac{4}{3}\mu_1\left(\frac{R_2}{R_0}\right)^3 \tag{64}$$

is the maximum value of pressure. A graph of $p(t')$ is shown in Fig. 7(c) for different values of the ratio R_2/R_0, in the absence of eruptions.

6 ERUPTIONS

The values of p_m shown in Fig. 7(c) are of the order of tens or hundreds of MPa, much greater than the critical pressure p_0 for eruption, that is typically smaller than 10 MPa. We assume that, when $p = p_0$, an eruption takes place through a tensile fracture connecting the magma chamber with the Earth's surface. During eruption, pressure in the chamber changes according to

$$\frac{\mathrm{d}p}{\mathrm{d}t} = k_1\rho_2(\Phi - \Psi), \tag{65}$$

where Ψ is the magma outflow rate, that is proportional to overpressure p according to

$$\Psi = \frac{k_2}{\rho_2}p, \tag{66}$$

where k_2 is a constant depending on the conduit geometry and on the rheology of magma (Dragoni & Piombo 2020).

Since Ψ is of the order of 10–100 m^3 s^{-1} in typical effusive eruptions, while Φ is of the order of 10^{-2}–10^{-1} m^3 s^{-1}, Φ can be neglected in eq. (65) that reduces to

$$\frac{\mathrm{d}p}{\mathrm{d}t} + \frac{p}{\tau} = 0, \tag{67}$$

where

$$\tau = \frac{1}{k_1 k_2}. \tag{68}$$

Eq. (67) was first proposed by Wadge (1981). If eruption starts at $t = t_1$, the solution is

$$p(t) = p_0 \mathrm{e}^{-(t-t_1)/\tau} \tag{69}$$

so that the waning time τ is representative of the duration of eruption. The volume of erupted magma is

$$V_e = \int_{t_1}^{\infty} \Psi(t)\, dt. \tag{70}$$

With eqs (66) and (69), the integration yields

$$V_e = \frac{\pi p_0}{\mu_1} R_0^3, \tag{71}$$

where eq. (62) has been used. Hence the size of the eruption depends mainly on the radius R_0 of the magma chamber. From eqs (71) and (64), V_e is a fraction of the bubble volume V_2 equal to

$$f = \frac{p_0}{p_m}. \tag{72}$$

Since $\tau \ll \tau_5$, eruption reduces the overpressure p to negligible values in a time much smaller than pulse duration τ_5. After eruption, magma inflow continues at a rate Φ and the critical pressure p_0 can be reached again, giving rise to a new eruption, and so on. The sequence of eruptions terminates when magma inflow ceases, at $t = t_0 + \tau_5$. Hence, according to the model, the arrival of a magma bubble can give rise to a sequence of n eruptions, with $n = [p_m/p_0]$, where brackets indicate the integer part of the ratio. The total erupted volume is then $V_t = nV_e \le V_2$.

7 DISCUSSION

Vicari *et al.* (2011) illustrated typical time histories of magma effusion rates on Mount Etna considering values of erupted magma volumes ranging from 30 to 200 $\times$ 10^6 m^3. According to eq. (71), if we take $\mu_1 = 10^{10}$ Pa and $p_0 = 10^7$ Pa, we obtain $V_e \simeq 25 \times 10^6$ m^3 if $R_0 = 2$ km and $V_e \simeq 85 \times 10^6$ m^3 if $R_0 = 3$ km.

In order to illustrate the model, we consider a chamber with radius $R_0 = 2$ km and centre at depth $z_0 = -5R_0$ and a bubble with radius $R_2 = 200$ m rising from a distance equal to $4R_0$ from the bottom of the chamber, along a path with incidence angle $\alpha = 0$. We assume a density difference $\rho_1 - \rho_2$ between solid rock and magma equal to 400 kg m^{-3} and an acceleration of gravity $g = 10$ m s^{-2}.

In Fig. 2, we assume that temperature T_1 at the base of the chamber is equal to 1273 K. Fig. 2(b) shows that there is a smooth variation in temperature along the bubble path, from 984 to 1273 K. This entails an initial increase in viscosity η_1, followed by a decrease by a factor of 50, with values ranging between 8 $\times$ 10^{13} and 2 $\times$ 10^{15} Pa s (Fig. 3a).

Bubble velocity $u(z_1)$ in the proximity of the magma chamber can be calculated from eq. (26) with $\eta_1 = \eta_1(z_1)$, yielding $u(z_1) \simeq$ 20 m a^{-1}. Along most of the path, bubble velocity u is about 1 m a^{-1} (Fig. 3b). As a consequence of the decrease in η_1, u increases by a factor of 30 in the last part of the path. Accordingly, the characteristic ascent time τ_2 decreases from about 500 to 20 a.

However, the increase in velocity is slow and corresponds to a very small acceleration, having only a small effect on the bubble traveltime $\bar{t}(z)$, as shown in Fig. 3(c). From eq. (29), the time $\bar{t}(z_1)$ taken to cover the distance $4R_0$ is quite long, of the order of 10^4 a, but the last kilometre is covered in less than 200 a. A remarkable fact is that magma viscosity η_2 has no effect on the dynamics both outside and inside the bubble, a consequence of the fact that $\eta_2 \ll \eta_1$.

As to forced convection in the bubble, eqs (32) and (33) show that magma velocity in streamlines is proportional to bubble velocity u. Hence, the mixing time τ_4 is inversely proportional to u and there is complete mixing after a bubble run equal to 10 R_2 or 2 km. Mixing tends to keep uniform temperature and viscosity inside the bubble.

The streamline length increases with increasing ξ_2, but Fig. 5(b) shows that magma flow is faster in longer streamlines, so that the traveltime for a complete loop is about the same for all streamlines. During most of the ascent path, where $u \simeq 1$ m a^{-1} and $\tau_2 \simeq 500$ a, eq. (47) yields $\tau_4 \simeq 2800$ a for most streamlines (Fig. 6). A much smaller value of τ_4, that is 100 a, is found in the proximity of the magma chamber, where $\tau_2 = 20$ a.

The flow rate into the magma chamber is an asymmetric pulse, as shown in Fig. 7(a). According to eqs (49) and (27), pulse duration τ_5 depends on bubble radius R_2, velocity u and incidence angle α. If $\alpha = 0$, τ_5 is equal to $2\tau_2$ calculated at the bottom of the magma chamber, that is about 40 a for the assumed values of R_2 and u. The average value of inflow rate is $V_2/\tau_5 = 0.03$ m^3 s^{-1}, with a peak value $\Phi_m = 0.06$ m^3 s^{-1} that is reached about 9 a from the beginning of inflow. These flow rates are several orders of magnitude lower than those from typical basaltic dikes (Peltier *et al.* 2007).

Larger values of bubble radius R_2 would produce higher bubble velocities according to eq. (26), showing that u is proportional to the square of R_2. For example, a bubble with $R_2 = 400$ m has an initial velocity $u \simeq 3$ m a^{-1}, reaching a value $u(z_1)$ as large as 80 m a^{-1} in the proximity of the chamber. The time $\bar{t}(z_1)$ taken to cover the distance $4R_0$ is four times smaller, that is about 3000 a. According to eq. (27), the characteristic ascent time τ_2 is inversely proportional to bubble radius R_2, a property that is shared with mixing time τ_4 and pulse duration τ_5. Therefore, τ_4 and τ_5 have halved values for a bubble with $R_2 = 400$ m, that is τ_4 varies from 1400 to 50 a and τ_5 is equal to 20 a.

A different value of temperature T_1 at the base of the magma chamber would not change sensibly this picture. For example, if we assume $T_1 = 1473$ K, viscosity η_1 at $z = z_1$ would be about 2 $\times$ 10^{13} Pa s, a factor of 0.2 smaller. This corresponds to a greater final velocity, that is $u(z_1) \simeq 100$ m a^{-1} if the bubble radius is R_2 = 200 m. Characteristic ascent time τ_2, mixing time τ_4 and inflow time τ_5 will be 0.2 times smaller, as well as the Maxwell time τ_1. In particular, τ_5 is equal to about 8 a, that is reduced by a further factor of 2 if $R_2 = 400$ m.

According to eq. (64), the maximum pressure p_m is proportional to the cube of the ratio R_2/R_0. Values of p_m for $R_2 = 200$, 300 and 400 m are about 13, 45 and 107 MPa, respectively (Fig. 7c). Since critical pressure values for eruption are of the order of 10 MPa, inflow of a magma bubble can produce an eruption far in advance that the maximum pressure p_m is attained.

Dragoni & Piombo (2020) considered the case in which the duration of magma pulse is comparable with the duration of eruption. Here, the case is considered of a much slower pulse that can produce several single eruptions according to the value of the ratio p_0/p_m. In the three cases shown in Fig. 7(c), the number n of eruptions would be equal to 1, 4 and 10, respectively, with total erupted volumes V_t equal to 25, 100 and 250 $\times$ 10^6 m^3.

8 CONCLUSIONS

The ascent of a spherical magma bubble through the low-viscosity region below a magma chamber has been considered. Under some simplifying assumptions, an analytical solution has been given, providing the upward magma flow and the associated dragging of surrounding crustal rocks. Magma volumes in the bubble have been assumed to be at least equal to magma batches in typical effusive

eruptions on Mount Etna, corresponding to bubble radii of a few hundred metres.

The ascent velocity of the bubble depends mainly on the bubble radius and the viscosity of surrounding rocks. It does not depend on the viscosity of magma, because it is much smaller than the viscosity of rocks. The high ambient temperature gives the bubble a velocity reaching tens of metres per year in the proximity of the chamber. It shows that the bubble can cover several kilometres with only moderate cooling.

An interesting aspect is that the magma in the bubble is subject to a forced convection. Analytical expressions for the streamlines in the bubble have been obtained and the traveltime of magma along streamlines has been calculated. It results in a mixing time of the order of few tens of years, contributing to keep a uniform temperature in the bubble.

Inflow of the bubble in the magma chamber produces a magma pulse and an overpressure in the chamber. Under reasonable assumptions, the pulse shape and duration have been calculated analytically as functions of the bubble radius, ascent velocity and incidence angle. Pulse duration can be several tens of years. The associated overpressure is an increasing function of time that may produce an eruption, if a critical pressure value is attained. Eruption releases a fraction of the magma contained in the bubble and reduces overpressure to zero. Continued magma inflow may produce a sequence of eruptions, ending when the entire bubble has entered the chamber.

Of course, this is a very simplified picture of more complex processes occurring below a magma chamber. Feeding of the chamber may be a combination of diapir, dike and porous flows. With regard to the first mechanism, the model shows that it may occur thanks to the rheological properties of the region below the chamber. A single bubble has been considered, but several bubbles with different sizes may contribute at the same time. The eruption mechanism has been simplified too. It was assumed that, in each eruption, effusion rate is controlled only by pressure decrease due to emptying of the magma chamber, while other processes occurring in the volcanic conduit may contribute (Piombo *et al.* 2016; Piombo & Dragoni 2021).

ACKNOWLEDGEMENTS

The author is grateful to Thierry Menand, Augusto Neri and an anonymous reviewer for constructive comments and suggestions on the first version of the paper. Many thanks also to the editors Gael Choblet and Juan Carlos Afonso for helpful suggestions.

DATA AVAILABILITY

There are no new data or code associated with this paper.

REFERENCES

Abramowitz, M. & Stegun, I.A., 1972. *Handbook of Mathematical Functions,* National Bureau of Standards.

Annen, C., 2011. Implications of incremental emplacement of magma bodies for magma differentiation, thermal aureole dimensions and plutonism–volcanism relationships, *Tectonophysics,* **500,** 3–10.

Batchelor, G.K., 1967. *An Introduction to Fluid Dynamics,* Cambridge Univ. Press.

Bons, P.D., Arnold, J., Elburg, M.A., Kalda, J., Soesoo, A. & van Milligen, B.P., 2004. Melt extraction and accumulation from partially molten rocks, *Lithos,* **78,** 25–42.

Burgisser, A. & Bergantz, G.W., 2011. A rapid mechanism to remobilize and homogenize highly crystalline magma bodies, *Nature,* **471,** 212–217.

Cashman, K.V., Sparks, R.S.J. & Blundy, J.D., 2017. Vertically extensive and unstable magmatic systems: a unified view of igneous processes, *Science,* **355**(6331), doi:10.1126/science.aag3055.

Crisp, J.A., 1984. Rates of magma emplacement and volcanic output, *J. Volc. Geotherm. Res.,* **20,** 177–211.

Currenti, G. & Bonaccorso, A., 2019. Cyclic magma recharge pulses detected by high-precision strainmeter data: the case of 2017 inter-eruptive activity at Etna volcano, *Sci. Rep.,* **9,** 7553, doi:10.1038/s41598-019-44066-w.

De Gori, P., Chiarabba, C. & Patanè, D., 2005. Q_p structure of Mount Etna: constraints for the physics of the plumbing system, *J. geophys. Res.,* **110,** B05303.

De Gori, P., Chiarabba, C., Giampiccolo, E., Martinez-Arèvalo, C. & Patanè, D., 2011. Body wave attenuation heralds incoming eruptions at Mount Etna, *Geology,* **39,** 503–506.

Degruyter, W. & Huber, C., 2014. A model for eruption frequency of upper crustal silicic magma chambers, *Earth planet. Sci. Lett.,* **403,** 117–130.

Del Negro, C., Currenti, G. & Scandura, D., 2009. Temperature dependent viscoelastic modeling of ground deformation: application to Etna volcano during the 1993–1997 inflation period, *Phys. Earth planet. Inter.,* **172**(3), 299–309.

Dragoni, M. & Piombo, A., 2020. A model for the effusion rate produced by a magma pulse, *Geophys. Res. Lett.,* **47,** e2019GL086193.

Gudmundsson, A., 2012. Magma chambers: formation, local stresses, excess pressures, and compartments, *J. Volc. Geotherm. Res.,* **237–238,** 19–41.

Karlstrom, L., Rudolph, M.L. & Manga, M., 2012. Caldera size modulated by the yield stress within a crystal-rich magma reservoir, *Nat. Geosci.,* **5,** 402–405.

Kirby, S.H. & Kronenberg, A.K., 1987. Rheology of the lithosphere: selected topics, *Rev. Geophys.,* **25**(6), 1219–1244.

Landau, L.D. & Lifshitz, E.M., 1987. *Fluid Mechanics,* 2nd edn, Pergamon Press.

Manea, V.C., Manea, M., Kostoglodov, V. & Sewell, G., 2005. Thermomechanical model of the mantle wedge in Central Mexican subduction zone and a blob tracing approach for the magma transport, *Phys. Earth planet. Inter.,* **149,** 165–186.

Menand, T., 2011. Physical controls and depth of emplacement of igneous bodies: a review, *Tectonophysics,* **500,** 11–19.

Menand, T., Annen, C. & de Saint Blanquat, M., 2015. Rates of magma transfer in the crust: insights into magma reservoir recharge and pluton growth, *Geology,* **43**(3), 199–202.

Michaut, C. & Jaupart, C., 2011. Two models for the formation of magma reservoirs by small increments, *Tectonophysics,* **500,** 34–49.

Newman, A., Dixon, T., Ofoegbu, G. & Dixon, J., 2001. Geodetic and seismic constraints on recent activity at Long Valley Caldera, California: evidence for viscoelastic rheology, *J. Volc. Geotherm. Res.,* **105**(3), 183–206.

Patanè, D., Barberi, G., Cocina, O., De Gori, P. & Chiarabba, C., 2006. Time-resolved seismic tomography detects magma intrusions at Mount Etna, *Science,* **313,** 821–823.

Paterson, S.R. & Vernon, R.H., 1995. Bursting the bubble of ballooning plutons: a return to nested diapirs emplaced by multiple processes, *Bull. geol. Soc. Am.,* **107,** 1356–1380.

Paterson, S.R., Okaya, D., Memeti, V., Economos, R. & Miller, R.B., 2011. Magma addition and flux calculations of incrementally constructed magma chambers in continental margin arcs: combined field, geochronologic and thermal modeling studies, *Geosphere,* **7,** 1439–1468.

Peltier, A., Staudacher, T. & Bachélery, P., 2007. Constraints on magma transfers and structures involved in the 2003 activity at Piton de La Fournaise from displacement data, *J. geophys. Res.,* **112**(B3), B03207.

Piombo, A. & Dragoni, M., 2021. Effusion rate from a volcanic conduit subject to pressure oscillations in a viscoelastic medium, *J. geophys. Res.,* **126,** e2020JB020642.

Piombo, A., Tallarico, A. & Dragoni, M., 2016. Role of mechanical erosion in controlling the effusion rate of basaltic eruptions, *Geophys. Res. Lett.,* **43,** 8970–8977.

Ranalli, G., 1995. *Rheology of the Earth,* Chapman and Hall.

Rubin, A.M., 1993. Dikes vs. diapirs in viscoelastic rock, *Earth planet. Sci. Lett.,* **119,** 641–659.

Scandone, R., Cashman, K.V. & Malone, S.D., 2007. Magma supply, magma ascent and the style of volcanic eruptions, *Earth planet. Sci. Lett.,* **253,** 513–529.

Schmeling, H., Cruden, A.R. & Marquart, G., 1988. Finite deformation in and around a fluid sphere moving through a viscous medium: Implications for diapiric ascent, *Tectonophysics,* **149,** 17–34.

Segall, P., 2016. Repressurization following eruption from a magma chamber with a viscoelastic aureole, *J. geophys. Res.,* **121,** 8501–8522.

Vicari, A., Ganci, G., Behncke, B., Cappello, A., Neri, M. & Del Negro, C., 2011. Near-real-time forecasting of lava flow hazards during the 1213 January 2011 Etna eruption, *Geophys. Res. Lett.,* **38,** L13317.

Wadge, G., 1981. The variation of magma discharge during basaltic eruptions, *J. Volc. Geotherm. Res.,* **11,** 139–168.

Weinberg, R.F. & Podladchikov, Y., 1994. Diapiric ascent of magmas through power law crust and mantle, *J. geophys. Res.,* **99,** 9543–9459.